


## Article

# Improving Hydrological Simulations with a Dynamic Vegetation Parameter Framework

Haiting Gu <sup>1</sup>, Yutai Ke <sup>2</sup>, Zhixu Bai <sup>2,3,4,5</sup> , Di Ma <sup>6,7,8,\*</sup>, Qianwen Wu <sup>2</sup>, Jiongwei Sun <sup>2</sup> and Wanghua Yang <sup>2</sup><sup>1</sup> Institute of Water Science and Engineering, Zhejiang University, Hangzhou 310058, China<sup>2</sup> College of Civil Engineering and Architecture, Wenzhou University, Wenzhou 325035, China; zhixu\_bai@wzu.edu.cn (Z.B.)<sup>3</sup> Key Laboratory of Engineering and Technology for Soft Soil Foundation and Tideland Reclamation of Zhejiang Province, Wenzhou 325035, China<sup>4</sup> Wenzhou Key Laboratory of Traffic Piezoelectric Engineering Technology, Wenzhou 325035, China<sup>5</sup> Zhejiang Collaborative Innovation Center of Tideland Reclamation and Ecological Protection, Wenzhou 325035, China<sup>6</sup> School of Civil Engineering, NingboTech University, Ningbo 315100, China<sup>7</sup> CAS Ningbo Beilun Institute of System Engineering, Ningbo 315800, China<sup>8</sup> College of Environmental Science and Engineering, Nankai University, Tianjin 300350, China

\* Correspondence: madi@nbt.edu.cn

**Abstract:** Many hydrological models incorporate vegetation-related parameters to describe hydrological processes more precisely. These parameters should adjust dynamically in response to seasonal changes in vegetation. However, due to limited information or methodological constraints, vegetation-related parameters in hydrological models are often treated as fixed values, which restricts model performance and hinders the accurate representation of hydrological responses to vegetation changes. To address this issue, a vegetation-related dynamic-parameter framework is applied on the Xinanjiang (XAJ) model, which is noted as Eco-XAJ. The dynamic-parameter framework establishes the regression between the Normalized Difference Vegetation Index (NDVI) and the evapotranspiration parameter K. Two routing methods are used in the models, i.e., the unit hydrograph (XAJ-UH and Eco-XAJ-UH) and the Linear Reservoir (XAJ-LR and Eco-XAJ-LR). The original XAJ model and the modified Eco-XAJ model are applied to the Ou River Basin, with detailed comparisons and analyses conducted under various scenarios. The results indicate that the Eco-XAJ model outperforms the original model in long-term discharge simulations, with the NSE increasing from 0.635 of XAJ-UH to 0.647 of Eco-XAJ-UH. The Eco-XAJ model also reduces overestimation and incorrect peak flow simulations during dry seasons, especially in the year 1991. In drought events, the modified model significantly enhances water balance performance. The Eco-XAJ-UH outperforms the XAJ-UH in 9 out of 16 drought events, while the Eco-XAJ-LR outperforms the XAJ-LR in 14 out of 16 drought events. The results demonstrate that the dynamic-parameter model, in regard to vegetation changes, offers more accurate simulations of hydrological processes across different scenarios, and its parameters have reasonable physical interpretations.

**Keywords:** Xinanjiang model; dynamic parameter; normalized difference vegetation index; evapotranspiration



**Citation:** Gu, H.; Ke, Y.; Bai, Z.; Ma, D.; Wu, Q.; Sun, J.; Yang, W. Improving Hydrological Simulations with a Dynamic Vegetation Parameter Framework. *Water* **2024**, *16*, 3335. <https://doi.org/10.3390/w16223335>

Academic Editor: Gordon Huang

Received: 16 October 2024

Revised: 16 November 2024

Accepted: 18 November 2024

Published: 20 November 2024



**Copyright:** © 2024 by the authors. Licensee MDPI, Basel, Switzerland. This article is an open access article distributed under the terms and conditions of the Creative Commons Attribution (CC BY) license (<https://creativecommons.org/licenses/by/4.0/>).

## 1. Introduction

Recent research indicates that since the end of the last century, vegetation ecology has exhibited varying trends across different regions [1]. The types and growth conditions of vegetation can alter the hydrological mechanisms, such as evapotranspiration and interception, and influence the water balance and runoff processes [2,3]. Although vegetation growth exhibits seasonal variation trends, the parameters closely related to vegetation remain at fixed values in most lumped hydrological models. This means that these models

cannot account for the response of hydrological processes to vegetation changes. Previous studies have highlighted that using fixed parameters in hydrological models can limit their simulation performance [4–6]. This calls for an eco-hydrological model with dynamic vegetation-related parameters that is capable of simulating the impact of vegetation changes on hydrological processes.

To improve the simulation accuracy of hydrological models, many researchers have employed hybrid methods to model watershed hydrological processes dynamically. Espinoza et al. [7] developed a hybrid model by coupling Long Short-Term Memory (LSTM) networks with the Simple Hydrological Model (SHM), showing that the hybrid model outperforms both the SHM and the LSTM individually. These models demonstrate that the improvement in accuracy stems from the dynamic parameters output by the LSTM. Similarly, Feng et al. [8] established a hybrid HBV model, which showed that the dynamic parameters  $\beta$  and  $\gamma$  allowed it to achieve a simulation performance comparable to that of the LSTM. Other researchers have also employed LSTM to incorporate dynamic parameters into hydrological models [9,10]. By leveraging deep learning black-box models such as LSTM, the hybrid models can achieve the dynamic parameterization of hydrological models without consideration of physical processes through loss-function minimization. At the same time, with hydrological models, hybrid models can still simulate reliable hydrological variables, even if these variables have not been trained in the models, which is not achievable with standalone black-box models [11]. While hybrid models significantly enhance the simulation capability of hydrological variables, they also increase model complexity, which is associated with the increasing uncertainty. This uncertainty manifests not only in the model's internal behavior but also in the parameters, particularly those with unclear physical mechanisms [12].

Another method for achieving model dynamization is to incorporate additional hydrometeorological and ecological data. For instance, the extra vegetation data, such as the Normalized Difference Vegetation Index (NDVI) or Leaf Area Index (LAI), provide a finer description of dynamic vegetation state variables, which indirectly dynamizes the model instead of modifying the fixed parameters directly. Jin et al. [13] modified the SWAT model using the high-resolution remote-sensing data of LAI, which solved the problem of LAI spatial discontinuity in the SWAT model. The Penman–Monteith (PM) formula has long been regarded as the most reliable method for estimating potential evapotranspiration in watersheds [14–17]. However, the PM formula cannot accurately partition evapotranspiration contributions between bare soil and vegetation. The impact of vegetation changes on watershed evapotranspiration is significant. For instance, during summer, increased root activity may enhance actual evapotranspiration due to enhanced water uptake, while drought can delay the recovery of water use efficiency [8]. To address this, Leuning et al. [18] improved the PM formula by incorporating LAI (PML formula) to separately calculate evapotranspiration contributions from bare soil and vegetation. Bai et al. [19] replaced the empirical evapotranspiration calculation formula with the PML formula in the Hydroinformatic modeling system (HIMS) model and found that the modified model showed a significant improvement in the streamflow and soil moisture simulations as compared to the original model. This is a reliable and interpretable approach, where hydrometeorological and ecological data are input into the model to correct the state variables based on equations derived from physical processes. However, this approach can only correct the state variables of the model and cannot utilize the dynamical parameters in the model. In reality, the vegetation changes in the hydrological processes are also reflected in model parameters, which controls the simulation of canopy interception, evapotranspiration, and rainfall infiltration [20–23].

Among various vegetation index, the Normalized Difference Vegetation Index (NDVI) effectively reflects the spectral, morphological, and environmental characteristics of vegetation across different types, seasons, and growth conditions [24]. Due to its versatility, the NDVI has been widely adopted by researchers [25–27]. In eco-hydrological models, vegetation-related parameters can be inferred by establishing a regression model with the

NDVI [28]. In this study, a regression relationship between the NDVI and the model parameters is established to achieve dynamic parameterization, ensuring the interpretability of dynamic parameters. This method not only fully reflects the vegetation changes within the watershed but also fully considers the dynamic changes of model parameters under vegetation changes. By establishing the regression relationships between the NDVI and vegetation-related hydrological model parameters, the method proposed in this study can effectively introduce dynamic parameters to hydrological models. It also provides a tool to explore the impacts of vegetation changes on a broader range of hydrological processes, extending beyond the rainfall–vegetation change–runoff relationship.

## 2. Study Area and Data

The Ou River is the second largest river in the Zhejiang Province, bounded by  $118^{\circ}45' E$ – $121^{\circ}00' E$  and  $27^{\circ}28' N$ – $28^{\circ}48' N$  (Figure 1). It traverses the mountainous region of southern Zhejiang and flows eastward into the East China Sea. The study area is the basin upstream of the Qingtian Hydrological Station, covering a drainage area of  $13,735 \text{ km}^2$ . It is characterized as a mountainous river basin in a subtropical monsoon climate zone, featuring significant elevation variations and dense forest cover [29]. The primary vegetation types include evergreen coniferous forests, broad-leaved forests, mixed coniferous and broad-leaved forests, and a substantial proportion of artificial vegetation [30].

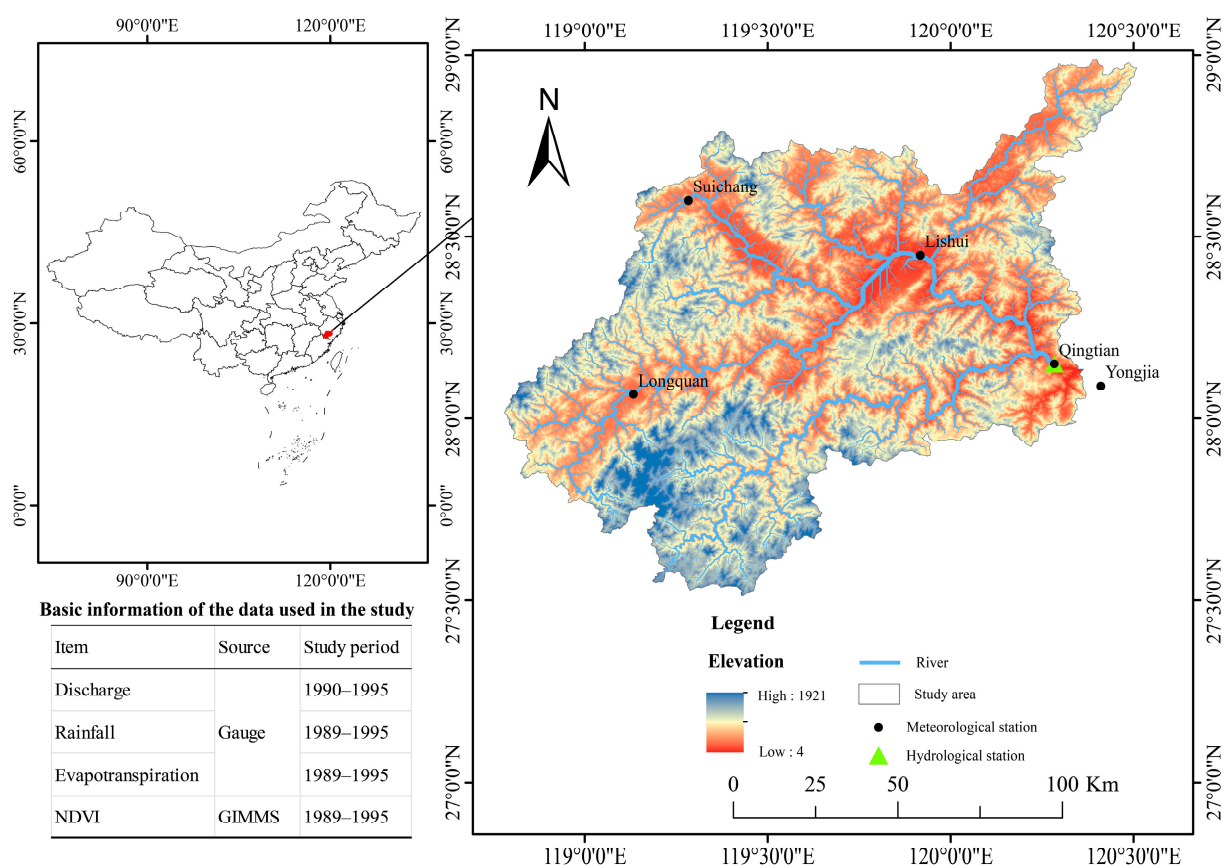


**Figure 1.** Location and basic information for the Ou River basin.

The gauged meteorological data for the operation of the hydrological model, including daily rainfall and evapotranspiration, are collected from five meteorological stations located in and around the Ou River basin as shown in Figure 1 (black points). Areal rainfall and evapotranspiration are calculated through the Thiessen polygon method. The observed discharge data for modeling covers the period from 1 January 1990 to 31 December 1995, as provided by the Qingtian Hydrological Station. This study also uses monthly NDVI data

from December 1989 to December 1995, which is sourced from the Global Inventory Modeling and Mapping Studies (GIMMS). The GIMMS NDVI dataset has a spatial resolution of  $8 \text{ km} \times 8 \text{ km}$  and a temporal resolution of 15 days [31]. The NDVI data is aggregated on a monthly scale. In this study, the calibration and validation periods for the hydrological models are 1990–1993 and 1993–1995, respectively.

### 3. Methods

Figure 2 shows the flowchart of this study. In this study, an eco-hydrological model based on the Xinanjiang (XAJ) model, called Eco-XAJ, is proposed, which incorporates vegetation change into the model using an NDVI regression module. Then, the discharge simulation performance of the Eco-XAJ model and the XAJ model is compared during the full period, the dry seasons, and the drought events in the Ou River basin.

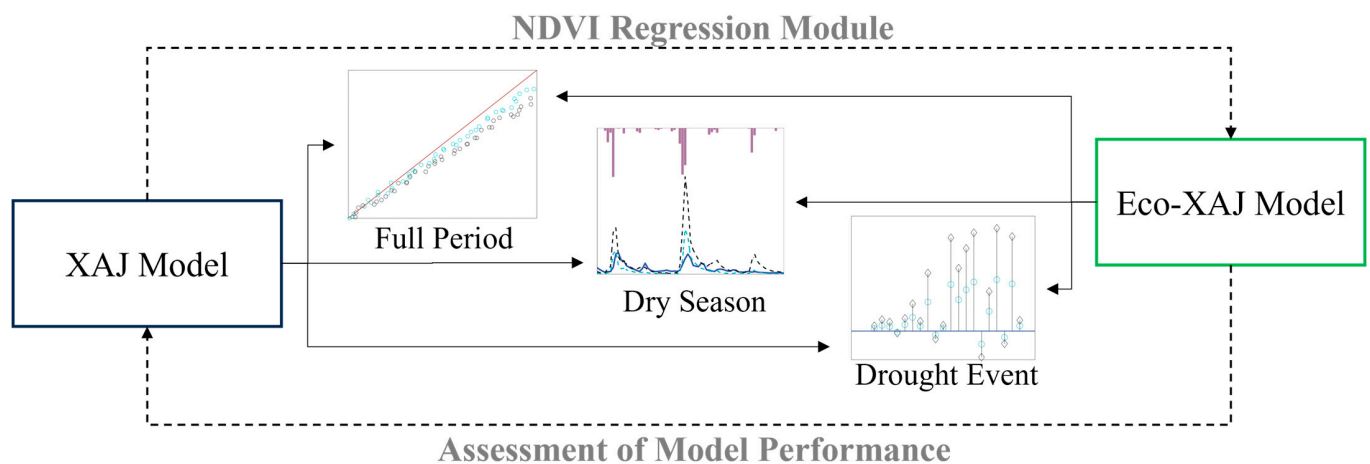


**Figure 2.** Flowchart of the study.

#### 3.1. Hydrological Model

The Xinanjiang (XAJ) model is a lumped hydrological model developed in the 1970s [32]. The XAJ model operates on a daily time step and is based on the principles of the water balance with four modules, including evapotranspiration, runoff generation, runoff separation, and routing. It divides the watershed into several sub-basins or hydrological response units, each of which is represented by a set of parameters that govern its hydrological behavior. The model is especially suitable for catchments in humid and semi-humid areas, where rainfall is often intense and variable. Key features of the XAJ model include its simplicity, its adaptability to different environmental conditions, and its ability to incorporate spatial variations in rainfall and other meteorological variables. It has been widely applied in flood forecasting, water resource management, and environmental studies, making it a critical tool for hydrologists and researchers seeking to understand and manage water systems in regions with diverse hydrological characteristics [33,34].

The unit hydrograph method is used as the routing modules in the XAJ model [32]. This method applies the unit hydrograph for surface runoff, while interflow and groundwater flow are routed through linear reservoirs. After routing to the outlet section, the results of the linear reservoir routing are combined with the unit hydrograph runoff, and the final simulated discharge at the catchment outlet is obtained. Another method is the Linear Reservoir method, where the surface runoff, interflow, and groundwater flow are all routed through linear reservoirs [33]. In order to determine the suitable runoff routing method for the study area, this study applies both the unit hydrograph method and the Linear Reservoir method to route the runoff generated by the XAJ model, referred to as XAJ-UH and XAJ-LR, respectively.

### 3.2. Dynamic Parameterization Considering Vegetation Changes

In the XAJ model, the conceptual parameter  $K$  directly affects the model's evapotranspiration, thereby influencing subsequent calculations of soil moisture and runoff generation. As shown in Equation (1),  $K$  is a correction factor from potential evapotranspiration to actual evapotranspiration:

$$E = K \times E_p \quad (1)$$

where  $E$  and  $E_p$  represent the actual evapotranspiration and potential evapotranspiration, respectively. Considering the impact of vegetation on evapotranspiration [35], the modified XAJ model assumes that the value of  $K$  is dynamic and related to the NDVI, in contrast to the original model where  $K$  is assumed to be a constant. Here, a regression relationship between  $K$  and the NDVI is established and then integrated into the XAJ model, which is referred to as the Eco-XAJ model.

### 3.3. Calibration and Evaluation of the Model

The parameters of the XAJ model are calibrated with the Non-Dominated Sorted Genetic Algorithm II (NSGA-II) [36,37]. A more detailed description of the model's calibration and sensitivity analysis has been provided by Liu et al. [33], and the basic information of parameters calibrated in our study is listed in Table A1.

Three objective functions are used in the model calibration, i.e., the Nash–Sutcliffe Efficiency coefficient ( $NSE$ ), the Correlation Coefficient ( $r$ ), and the Percent Bias ( $pBIAS$ ).

$$NSE = 1 - \frac{\sum_{i=1}^N (y_i - \hat{y}_i)^2}{\sum_{i=1}^N [y_i - \bar{y}]^2} \quad (2)$$

$$r = \frac{\sum_{i=1}^N [\hat{y}_i - \bar{\hat{y}}][y_i - \bar{y}]}{\sqrt{\sum_{i=1}^N [\hat{y}_i - \bar{\hat{y}}]^2 \sum_{i=1}^N [y_i - \bar{y}]^2}} \quad (3)$$

$$pBIAS = \frac{\sum_{i=1}^N \hat{y}_i - y_i}{\sum_{i=1}^N y_i} \times 100\% \quad (4)$$

where  $y_i$  is the observed value,  $\hat{y}_i$  is the simulated value,  $\bar{y}$  is the mean value of observation, and  $\bar{\hat{y}}$  is the mean value of simulation. According to the definition, when  $NSE$  and  $r$  approach 1 and  $pBIAS$  approaches 0, it indicates that the model simulation is more accurate. In this study,  $NSE$  and  $r$  are used to evaluate simulation performance.  $NSE$  also serves as the basis for filtering parameter  $K$ .  $r$  is employed to explain the linear correlation between the monthly optimal parameter  $K$  and the NDVI, as well as between the dynamic parameter  $K$  and the monthly optimal parameter  $K$ .  $pBIAS$  is used to assess the model's performance in simulating the water balance.

For the Eco-XAJ model, a two-step calibration method is used. The first step involves calibrating the static model parameters, which is consistent with the XAJ model. The second step is to calibrate the dynamic parameter  $K$ . Figure 3 shows the procedure for building the Eco-XAJ model. The specific steps are as follows:

First, calculate the optimal value for each month. The optimal value of  $K$  for each month is determined through a traversal with the range set from 0.01 to 7. The remaining model parameters are set as the parameters calibrated in the original model. The parameter  $K$  corresponding to the best simulation performance (i.e., the maximum  $NSE$ ) is selected for each month.

Second, select the effective optimal  $K$ . When the XAJ model performs poorly in the simulation due to the limitation of the model structure or because of forcing the data quality, there may be months in which no reasonable simulation results can be obtained, regardless of the changes in parameter  $K$ . The optimal  $K$  values for these months are treated as anomalies. To avoid the influence of these anomalies, they are excluded based on the following three criteria: (1) the optimal  $K$  value for a month falls at the boundary of the

specified range; (2) the observed discharge during a month does not align with rainfall patterns; and (3) there is a poor simulation performance during a month, characterized by a substantial deviation between the simulated and observed discharges.

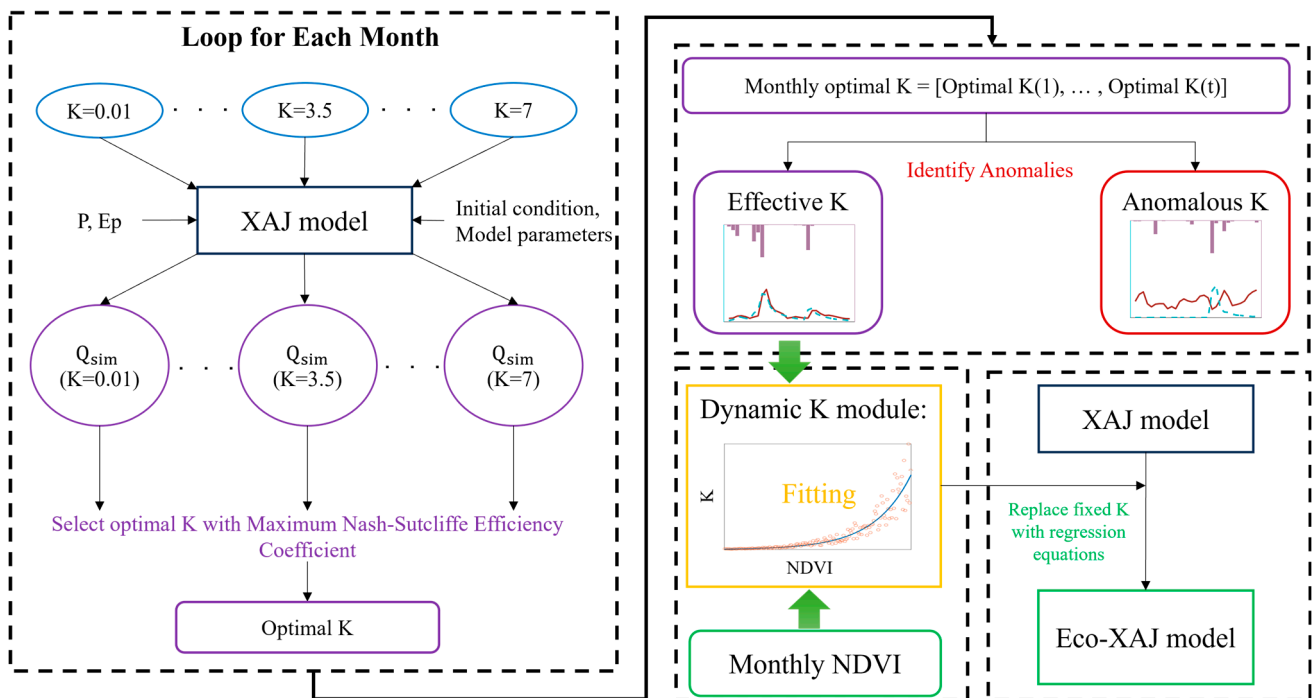


Figure 3. Procedure of building the Eco-XAJ model.

Third, build the dynamic K module. The dynamic K module is built based on the regression relationship between the monthly optimal K parameters and the monthly NDVI sequence. This study also considers the potential lagged effects of the vegetation changes on watershed hydrological processes. Therefore, there are two fitting approaches: (1) fitting the optimal K parameter for the current month with the NDVI of the current month (Lag-0 model) and (2) fitting the optimal K parameter for the current month with the NDVI of the previous month (Lag-1 model). The regression equations derived from the fitting process can calculate the dynamic parameter K, taking the vegetation changes into consideration. Subsequently, replacing the fixed parameter K in the XAJ model with this dynamic parameter K completes the modeling process of Eco-XAJ.

Finally, construct the Eco-XAJ model. The fixed K in the XAJ model is replaced with the NDVI to solve K regression equation in the XAJ model.

#### 4. Results and Discussion

##### 4.1. The Relationship Between K and the NDVI

Figure 4 shows the relationship between the NDVI and the optimal values of K for the same month, as well as the relationship between the current month’s K and the previous month’s NDVI. The calibration and validation results for the XAJ models can be found in Table A2. According to Figure 4, for both XAJ-UH and XAJ-LR, K and the NDVI exhibit an exponential relationship. However, the XAJ-LR model shows a more pronounced exponential relationship between K and the NDVI. Additionally, compared to XAJ-UH, XAJ-LR generally shows a stronger correlation between K and the NDVI within the same month. Furthermore, the distribution range of K in the XAJ-LR is broader as compared to the XAJ-UH, with fewer values concentrated between 0.01 and 1. Compared with the XAJ-UH model, the K values in the XAJ-LR model are more concentrated around the upper boundary of 7 rather than the lower boundary of 0.01.

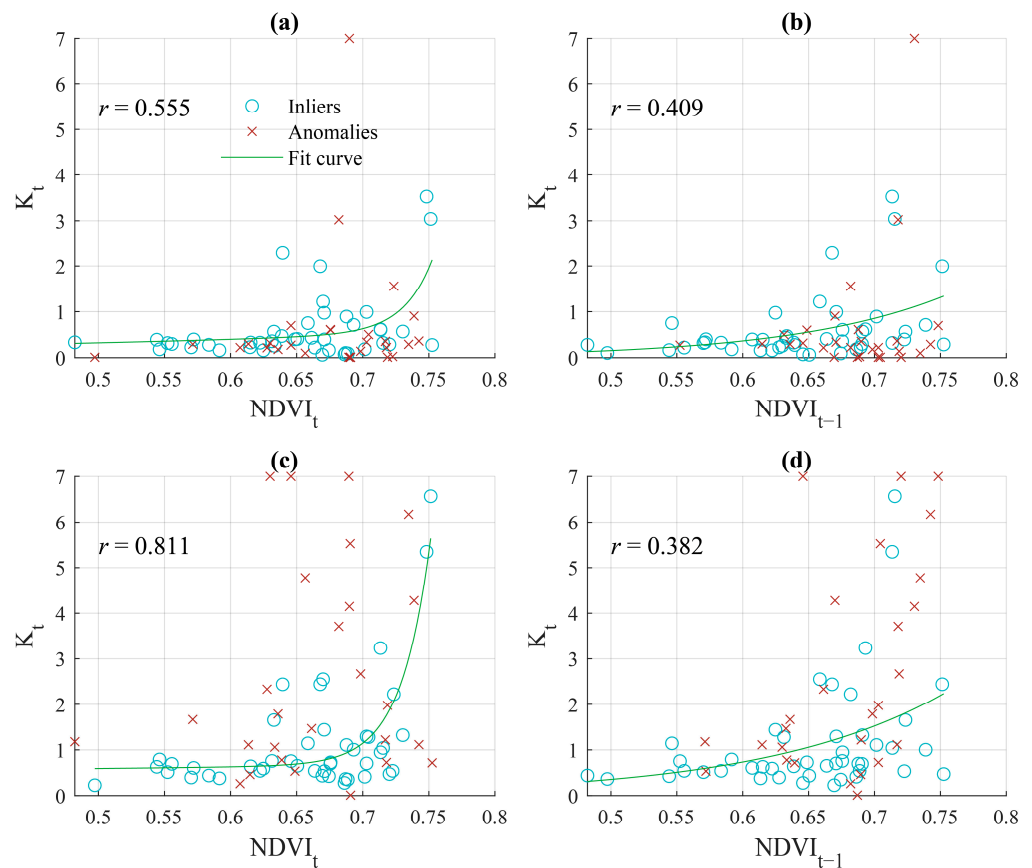


**Figure 4.** Scatter plot of  $K$  and the NDVI: (a,b) represent the XAJ-UH model and (c,d) represent the XAJ-LR model.  $NDVI_t$  and  $K_t$  indicate the relationship for the same month;  $NDVI_{t-1}$  and  $K_t$  indicate the relationship with a one-month lag.

For the XAJ-UH, the regression equation for estimating  $K$  in the same month using the same month's NDVI is shown in Equation (5). The regression equation for estimating the current month's  $K$  using the previous month's NDVI is shown in Equation (6). For the XAJ-LR, the regression equation for estimating  $K$  in the same month using the same month's NDVI is shown in Equation (7). The regression equation for estimating the current month's  $K$  using the previous month's NDVI is shown in Equation (8).

$$K_t = 0.1133e^{2.093NDVI_t} + 1.134 \times 10^{-15}e^{46.34NDVI_t} \quad (5)$$

$$K_t = 2.162 \times 10^{-3}e^{8.544 \times NDVI_{t-1}} \quad (6)$$

$$K_t = 0.455e^{0.526NDVI_t} + 8.996 \times 10^{-15}e^{45.17NDVI_t} \quad (7)$$

$$K_t = 9.17 \times 10^{-3}e^{7.305NDVI_{t-1}} \quad (8)$$

As indicated by the  $r$  values in Figure 4a,c, it is evident that, either using XAJ-UH or XAJ-LR, the fitted curve based on the  $K$  and the NDVI of the same month demonstrates a stronger correlation. It makes sense that  $K$  increases with the rise in the NDVI. When the NDVI is low, the vegetation in the watershed is not abundant, so the amount of water absorbed by the roots and transpired by the vegetation is also low. Conversely, high values of the NDVI indicate dense vegetation in the watershed, and a large amount of water transpired by the vegetation. The result is consistent with several previous research findings, which indicate that evapotranspiration increases with vegetation greening [38].

Additionally, Figure 4a,c exhibits a shared trend: the fitted curves show an inflection point around an NDVI of approximately 0.68, where the K values start to rise sharply. In contrast, the fitted curves in Figure 4b,d do not display such a pronounced inflection point.

#### 4.2. Simulation Performance of Full Period

The four regression equations are used to build the Eco-XAJ model, where Equations (5) and (6) are used in XAJ-UH, noted as Eco-XAJ-UH with the Lag-0 module and Eco-XAJ-UH with the Lag-1 module, and Equations (7) and (8) are used in XAJ-LR, noted as Eco-XAJ-LR with the Lag-0 module and Eco-XAJ-LR with the Lag-1 module. The simulation results of the Eco-XAJ models and the original XAJ models from January 1990 to December 1995 are compared in Table 1. In Table 1, the best-performing Eco-XAJ model is highlighted in bold. According to Table 1, the Eco-XAJ-UH models with both the Lag-0 and Lag-1 modules outperform the XAJ-UH model, while the Eco-XAJ-LR model with the Lag-0 module performs better than the XAJ-LR model. The Eco-XAJ-UH with the Lag-0 module shows the best performance of all six models. Three of the four Eco-XAJ models perform better than the original models. Because the Eco-XAJ models with the Lag-0 module outperform those with the Lag-1 module, the subsequent analysis focuses on the Eco-XAJ models with the Lag-0 module.

**Table 1.** Comparison between the Eco-XAJ model and the XAJ model.

Model	NSE	<i>r</i>
XAJ-UH	0.635	0.799
Eco-XAJ-UH with Lag-0 module	<b>0.647</b>	<b>0.815</b>
Eco-XAJ-UH with Lag-1 module	0.639	0.815
XAJ-LR	0.589	0.768
Eco-XAJ-LR with Lag-0 module	<b>0.599</b>	<b>0.777</b>
Eco-XAJ-LR with Lag-1 module	0.565	0.767

Note: The best-performing model is highlighted in bold.

Figures 5 and 6 present the hydrographs simulated by Eco-XAJ-UH and Eco-XAJ-LR with the Lag-0 module. Three representative periods are selected, i.e., early May 1990 to early September 1990 (Duration I), early July 1991 to late December 1991 (Duration II), and early July 1995 to late December 1995 (Duration III). The periods of Duration I to III correspond to the wet season, the dry season and the recession periods, respectively. In Duration I, both Eco-XAJ-UH and Eco-XAJ-LR underestimate the flood peaks. The Eco-XAJ-LR model underestimates floods more significantly than the Eco-XAJ-UH model. As shown in Figure 6b, the three flood peaks exceeding 2000 m<sup>3</sup>/s, simulated by the Eco-XAJ-LR model before 1 July 1990, are all lower than those simulated by the XAJ-LR model. However, when the observed discharge is below 2000 m<sup>3</sup>/s, the simulations of the Eco-XAJ models are generally better than those of the original XAJ models. Specifically, the XAJ-LR model incorrectly simulates the flood peak on 3 July 1990, while the Eco-XAJ-LR simulates the discharge closer to the observation.

According to Figures 5c and 6c, the XAJ models overestimate the flood peaks in Duration II. The Eco-XAJ models address this issue, mainly due to their ability to simulate more accurate evapotranspiration. According to Figures 5d and 6d, there are several short rainfall events within the recession process in Duration III. It can be observed that the discharge does not show a significant flood peak despite the rainfall reaching its peak. The XAJ models present incorrect flow peaks for all these rainfall events, while the Eco-XAJ models almost perfectly reproduce the variations of discharge during this period, with only one incorrect flow peak. For the rainfall events less than 100 mm, the XAJ models and the Eco-XAJ models incorrectly simulate the flood peaks, but the flood peaks simulated by Eco-XAJ are lower than those of the original model.



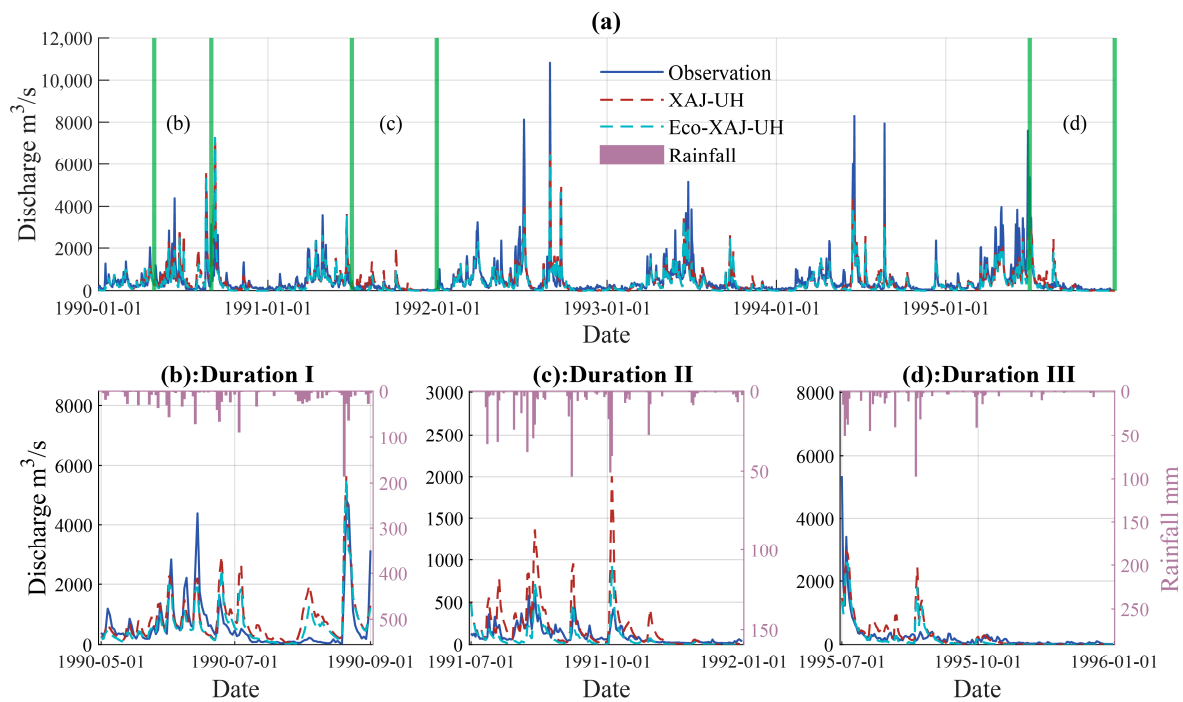


**Figure 5.** Hydrograph of the Eco-XAJ-UH model in (a) the full period, (b) Duration I (the wet season), (c) Duration II (the dry season), and (d) Duration III (the recession periods).

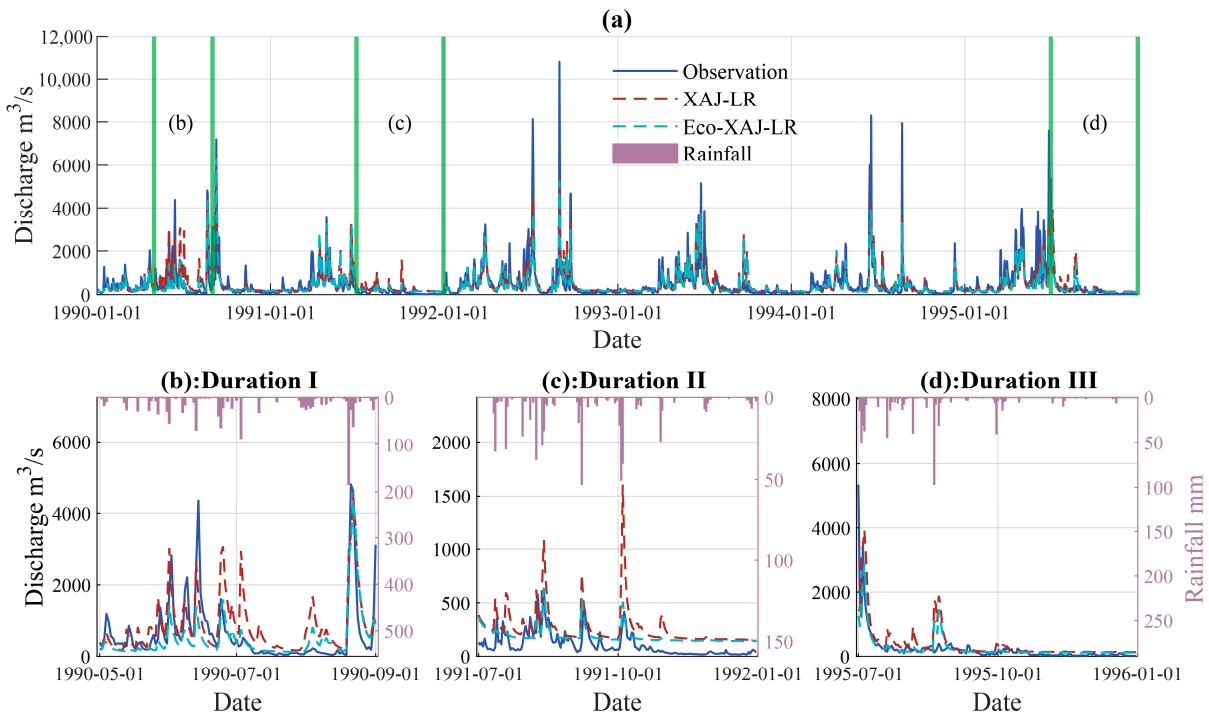


**Figure 6.** Hydrograph of the Eco-XAJ-LR model in (a) the full period, (b) Duration I (the wet season), (c) Duration II (the dry season), and (d) Duration III (the recession periods).

To better visualize the differences between the models, the simulation results of the Eco-XAJ and XAJ models are presented in Figure 7. In Figure 7a, the Eco-XAJ model's scatter points are more concentrated around the 1:1 line, indicating that the simulated discharge of the Eco-XAJ-UH model is closer to the observed discharge, as compared to the original model, when the observed discharge is less than 2000 m<sup>3</sup>/s. In Figure 7a, it can be observed that

the outliers primarily occur when the discharge exceeds 2000 m<sup>3</sup>/s, where the XAJ model underestimates the flood peak. This is consistent with the results shown in Figure 5a. In Figure 7b, it can be observed that the maximum deviation of discharge between the Eco-XAJ-UH model and the original model is approximately −1000 m<sup>3</sup>/s, when the discharge is less than 2000 m<sup>3</sup>/s. As the simulated discharge of the original model exceeds 2000 m<sup>3</sup>/s, the tendency for the Eco-XAJ-UH model to simulate lower discharges, as compared to the original model, gradually diminishes. When the simulated discharge of the original model surpasses 4000 m<sup>3</sup>/s, the simulated discharge of the Eco-XAJ-UH model becomes nearly identical to that of the original model. This indicates that the Eco-XAJ-UH model almost does not reduce the original model's flood-peak simulation performance. The comparison between the Eco-XAJ-LR model and the XAJ-LR model is shown in Figure 7c,d. The conclusions drawn with Eco-XAJ-LR model are similar to those drawn with the Eco-XAJ-UH model. According to Figure 7b,d, when the discharge is below 3000 m<sup>3</sup>/s, the difference between the Eco-XAJ-LR and the XAJ-LR models is more significant than that between the Eco-XAJ-UH and XAJ-UH models, with the maximum deviation being around −2250 m<sup>3</sup>/s. This deviation mainly occurs during the wet seasons, as shown in Figure 6b. In Duration I, the XAJ-LR model overestimates the discharge, while the simulation of Eco-XAJ-LR model closely matches the observation. This indicates that the improvement in the evapotranspiration process in the Eco-XAJ model effectively enhances the model's simulation performance.

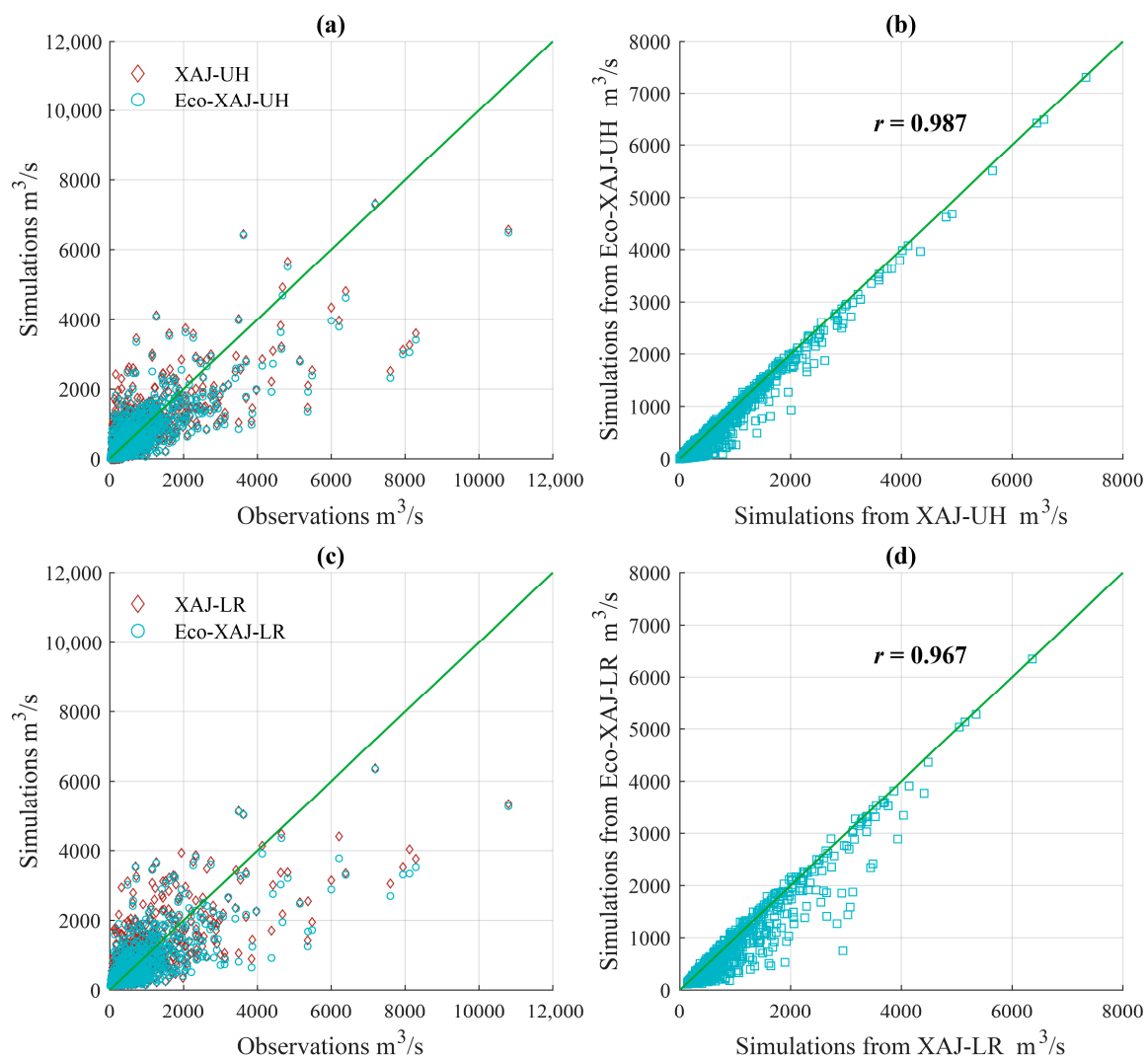


**Figure 7.** Comparison of the simulation (a,b) between the XAJ-UH model and the Eco-XAJ-UH model, and (c,d) between the XAJ-LR model and the Eco-XAJ-LR model.

For a more detailed analysis, the error plots of the Eco-XAJ model corresponding to the observed discharges are presented in Figure 8. Figure 8a,c illustrates the fact that when the observed discharge is below approximately 1000 m<sup>3</sup>/s, the absolute error of the Eco-XAJ model is generally lower than that of the XAJ model. As shown in Figure 8b,d, the error analysis of the discharge less than 1000 m<sup>3</sup>/s is conducted, where a  $\Delta\text{Error}$  greater than 0 indicates that the Eco-XAJ model outperforms the XAJ model. The red solid line shows the cumulative  $\Delta\text{Error}$ . If the slope of the cumulative  $\Delta\text{Error}$  is greater than 0, it indicates that the advantage of the Eco-XAJ model is increasing. According to Figure 8b,d, it is evident that the difference between the Eco-XAJ-LR and XAJ-LR models is more pronounced as compared to that between Eco-XAJ-UH and XAJ-UH. The cumulative  $\Delta\text{Error}$  in Figure 8d is approximately twice that shown in Figure 8b. This indicates that the improvement in the simulation accuracy of Eco-XAJ-LR is greater than that of Eco-XAJ-UH. Furthermore, both subplots reveal that the advantage of the Eco-XAJ models increases with discharge ranging from 0 m<sup>3</sup>/s to 600 m<sup>3</sup>/s. However, in the range of the discharge from 600 m<sup>3</sup>/s to 1000 m<sup>3</sup>/s, the slope is approximately 0, suggesting that the advantage of the Eco-XAJ models weakens.

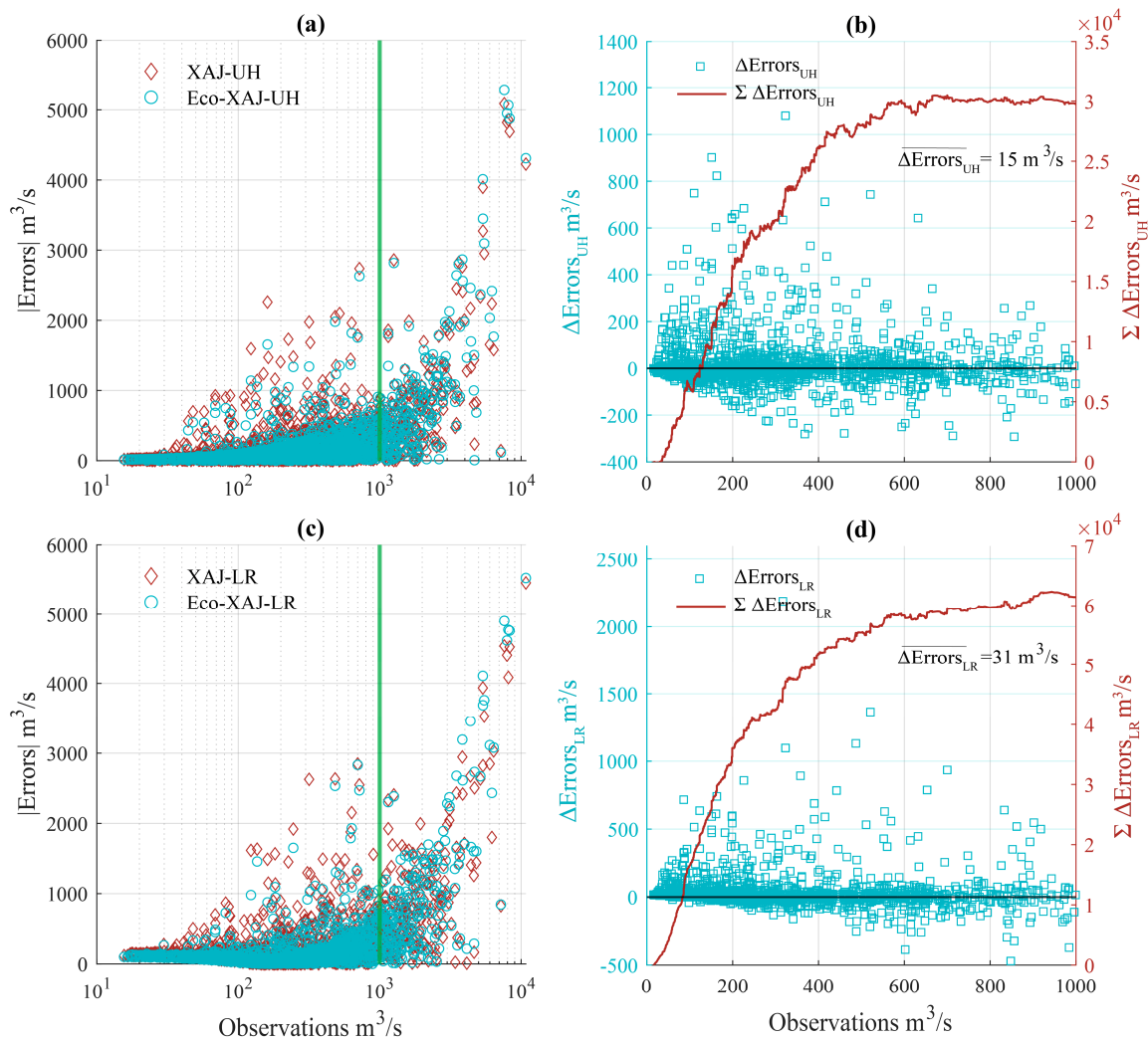


**Figure 8.** (a,c) are scatter plots of corresponding discharge errors, while (b,d) show scatter plots and the cumulative  $\Delta\text{Error}$  when the observed discharge is below 1000 m<sup>3</sup>/s, where  $\Delta\text{Error} = |\text{Error}_{\text{XAJ}}| - |\text{Error}_{\text{Eco-XAJ}}|$  and  $\overline{\Delta\text{Error}}$  is the mean value of  $\Delta\text{Error}$ .

#### 4.3. Simulation Performance During Dry Seasons

The hydrographs during the dry seasons (from October to February) are shown in Figures 9 and 10, in which the advantages and limitations of the Eco-XAJ models are

demonstrated. The Eco-XAJ model also exhibits notable improvements, especially in correcting the XAJ model's overestimation of peak discharges. For example, the XAJ models significantly overestimate the peak on 5 October 1991, 10 November 1993, and 12 October 1994, but the Eco-XAJ models successfully mitigate this overestimation, and the Eco-XAJ-LR model shows the most significant improvement and provides the best match for the observed discharge. When the XAJ models fail to simulate the discharge, the improvement of the Eco-XAJ models is also limited. In the dry seasons of 1990 and 1992, both the original XAJ models and the Eco-XAJ models are not able to simulate the peak discharge accurately. In the dry season, the Eco-XAJ models' runoff simulation performances generally improve. However, in a few cases, due to the poor performance of the original XAJ models, Eco-XAJ does not show significant improvements in the discharge simulation.

To quantitatively analyze the simulation performance of the models during the dry seasons, the *NSE* and *pBIAS* values for all models are listed in Table 2. It is observed that all four models have negative *NSE* values and large *pBIAS* values during the dry seasons in 1992, suggesting a poor performance of the XAJ and Eco-XAJ models, while all models perform well in 1994. The Eco-XAJ-UH model demonstrates the best *NSE* among the four models during the dry seasons in 1991, 1993, and 1994. Notably, in 1991, Eco-XAJ-UH also achieves the best *pBIAS*. As analyzed earlier, the Eco-XAJ-UH model exhibits superior peak simulation performance as compared to XAJ-UH, avoiding erroneous peaks that do not align with the observed discharge (around 1 November 1991), which contributes to its higher *NSE*. Furthermore, during the period between 5 October 1991 and 6 January 1992, the Eco-XAJ-UH model simulates a discharge that is closely aligned to the observation, leading to its top *pBIAS* performance. In 1994, the *NSE* for Eco-XAJ-UH improves slightly by 0.023 as compared to XAJ-UH, reflecting its success in addressing peak overestimation. The Eco-XAJ-LR model achieves the best *pBIAS* among the four models during the dry seasons in 1990, 1992, and 1994. However, as previously noted, the simulated hydrographs of all models in 1990 and 1992 are not reasonable. In 1994, similar to the Eco-XAJ-UH model, the Eco-XAJ-LR model shows a slight *NSE* improvement (0.028) as compared to XAJ-LR, which is also due to its success in addressing peak overestimation, resulting in its optimal *pBIAS*. In 1991, the Eco-XAJ models significantly surpass the XAJ models in both *NSE* and *pBIAS* due to the successful correction of the overestimation of peak discharge.

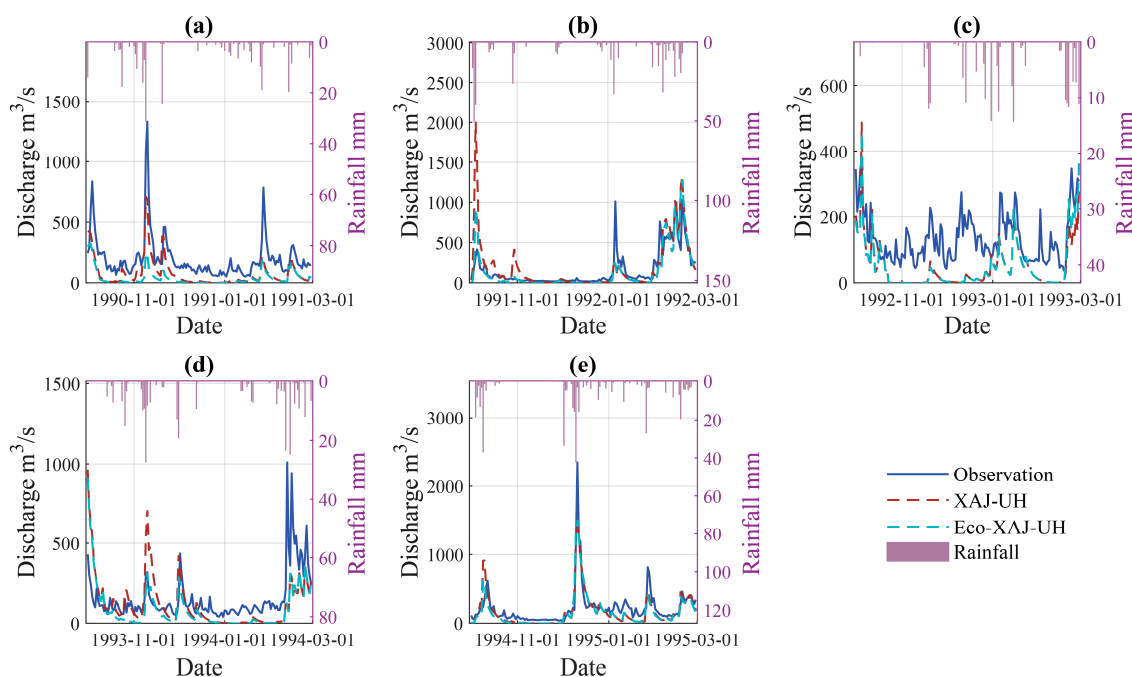


**Figure 9.** Hydrograph of Eco-XAJ-UH and the original model during the dry seasons of (a) 1990, (b) 1991, (c) 1992, (d) 1993, and (e) 1994.

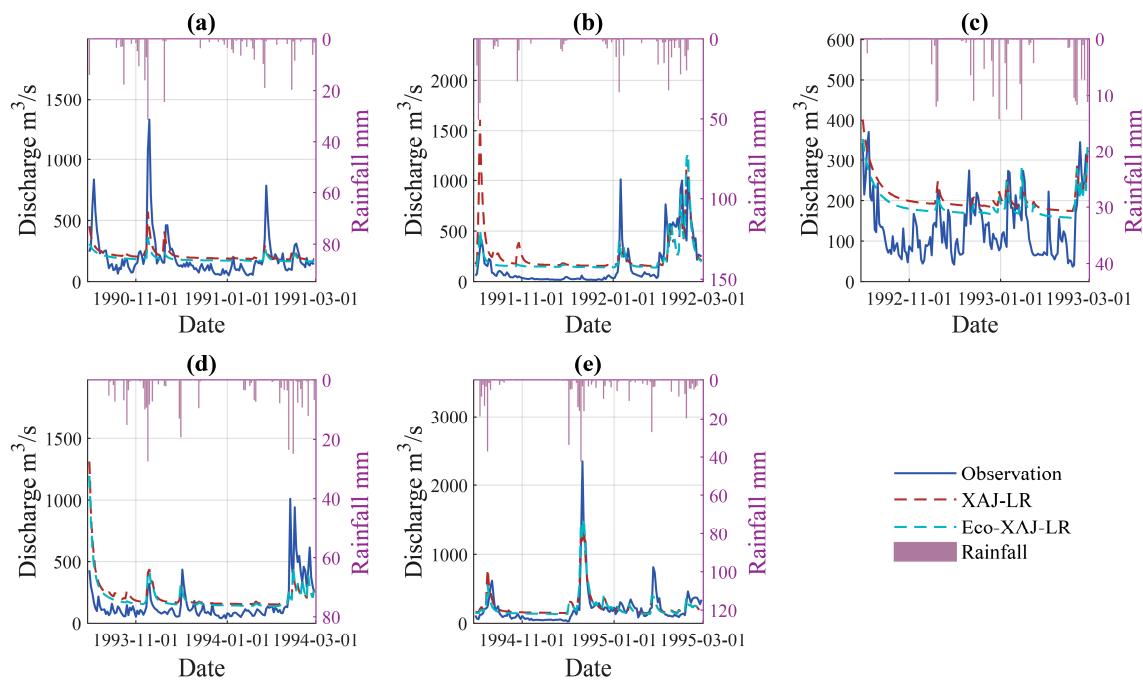


**Figure 10.** Hydrograph of Eco-XAJ-LR and the original model during the dry seasons of (a) 1990, (b) 1991, (c) 1992, (d) 1993, and (e) 1994.

**Table 2.** NSE and *pBIAS* during the dry seasons.

Metric	Model	1990	1991	Period 1992	1993	1994
NSE	Eco-XAJ-UH	−0.387	<b>0.616</b>	−1.027	−0.054	<b>0.726</b>
	Eco-XAJ-LR	0.225	0.511	−0.222	−0.072	0.682
	XAJ-UH	0.213	−0.020	−1.033	−0.210	0.703
	XAJ-LR	<b>0.343</b>	0.058	−0.669	−0.310	0.654
<i>pBIAS</i> %	Eco-XAJ-UH	−80.3	−14.2	−63.0	−43.5	−28.3
	Eco-XAJ-LR	−3.5	35.1	<b>42.4</b>	32.4	<b>6.9</b>
	XAJ-UH	−61.4	20.2	−63.9	−21.9	−19.8
	XAJ-LR	10.8	61.6	55.8	43.2	12.6

Note: The best-performing model is highlighted in bold.

#### 4.4. Simulation Performance of Drought Events

Considering that water balance is more critical during drought events, *pBIAS* is used as the evaluation metric for discharge in drought events. In this study, drought events are defined as events with a peak discharge of  $400 \pm 80 \text{ m}^3/\text{s}$  during a 20-day period. Table 3 lists the *pBIAS* for Eco-XAJ and XAJ in 16 drought events, along with the NDVI values. In Table 3, the better *pBIAS* values for specific events are highlighted in bold. The Eco-XAJ-UH outperforms the XAJ-UH in 9 out of 16 events, while the Eco-XAJ-LR outperforms the XAJ-LR in 14 out of 16 events. This indicates that dynamic parameterization can improve the model’s performance in simulating discharge in drought events. Moreover, it is also observed that Eco-XAJ-LR has more advantages than Eco-XAJ-UH in simulating discharge in drought events. Table 3 also shows that  $\Delta pBIAS$  ranges from 0 to −33.8% in the seven drought events, whereas the Eco-XAJ-UH model does not show improvement. This means that although Eco-XAJ-UH does not always outperform XAJ-UH in water-balance simulation, the performance gap is relatively small.

**Table 3.** *pBIAS* Comparison of the Eco-XAJ models and the original model during low-flow rainfall events.

Durations	<i>pBIAS</i> %				NDVI
	Eco-XAJ-UH	Eco-XAJ-LR	XAJ-UH	XAJ-LR	
1990-11-17–1990-12-07	−87.0	−8.7	−53.2	11.5	0.7202, 0.6895
1991-06-25–1991-07-15	<b>94.4</b>	<b>143.3</b>	132.1	173.7	0.6700, 0.7388
1991-07-15–1991-08-04	−72.5	<b>19.4</b>	72.5	90.3	0.7388, 0.6931
1991-08-24–1991-09-13	−44.4	<b>25.2</b>	<b>18.6</b>	56.5	0.6931, 0.7134
1991-10-03–1991-10-23	<b>17.0</b>	<b>38.4</b>	172.5	176.6	0.7483
1992-01-11–1992-01-31	−58.5	<b>75.5</b>	−56.2	90.3	0.6334
1993-02-14–1993-03-06	−25.3	−0.9	−44.7	3.9	0.4822, 0.5836
1993-08-13–1993-09-02	−91.6	−15.9	−67.1	<b>1.5</b>	0.7179, 0.6819
1993-11-21–1993-12-11	−45.6	<b>31.0</b>	−16.3	37.5	0.6328, 0.6613
1994-07-19–1994-08-08	−0.2	<b>47.0</b>	47.3	78.1	0.6877, 0.6755
1994-12-26–1995-01-15	−43.7	−5.1	−45.9	−4.2	0.5556, 0.6637
1995-02-04–1995-02-24	−20.9	−0.8	−7.2	2.4	0.6505
1995-07-14–1995-08-03	−29.0	−10.9	91.3	82.1	0.7303, 0.6899
1995-08-03–1995-08-23	<b>24.6</b>	<b>47.3</b>	126.1	141.3	0.6899
1995-08-23–1995-09-12	<b>23.5</b>	<b>51.3</b>	46.7	94.9	0.6899, 0.7171
1995-09-12–1995-10-02	−70.2	<b>34.9</b>	−57.8	65.7	0.7171, 0.7425

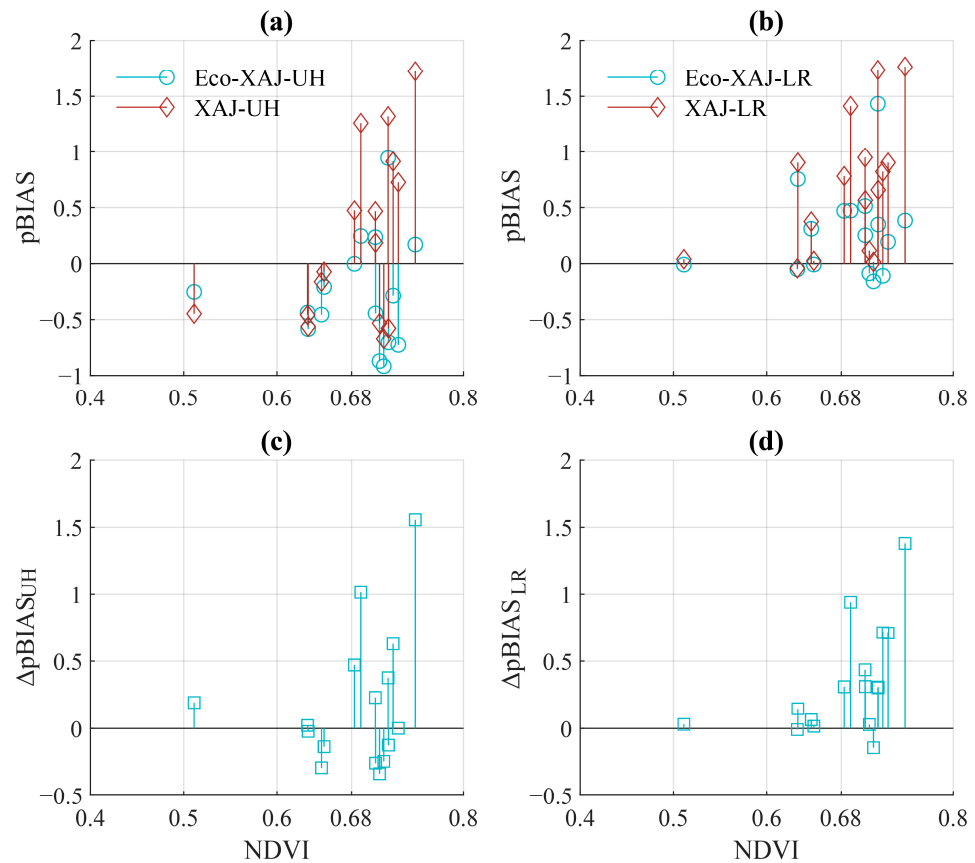
Note: The best-performing model is highlighted in bold.

Figure 11 illustrates the relationship between the NDVI and the model's performance during drought events. As shown in Figure 11a, the *pBIAS* values of the XAJ-UH model are negative when the NDVI is below 0.68 but become mainly positive when the NDVI exceeds 0.68. In contrast, the *pBIAS* values of the Eco-XAJ-UH model are mostly negative, with positive *pBIAS* values only occurring when the NDVI is greater than 0.68. Figure 11b shows that the *pBIAS* values for both the XAJ-LR and Eco-XAJ-LR models are generally positive. When the NDVI is below 0.68, the *pBIAS* values of the two models are similar. However, when the NDVI surpasses 0.68, a significant difference emerges between the models, with the *pBIAS* of the Eco-XAJ-LR model moving closer to zero. Figure 11a,b reveals that the XAJ-UH and XAJ-LR models produce relatively large *pBIAS* values when the NDVI exceeds 0.68. This suggests that the XAJ models face challenges in simulating the water balance accurately during drought events with high NDVIs.

Figure 11c,d, indicates that the Eco-XAJ model outperforms the XAJ model in a simulation in which the value on the vertical axis is greater than 0. Conversely, if the value is less than or equal to 0, it suggests that there is no improvement. As shown in Figure 11c, in cases where the model's performance improves, the magnitude of the improvement is greater than the magnitude of the decline observed in cases where the performance does not improve. It suggests that the Eco-XAJ-UH model generally performs better than the XAJ-UH model. Furthermore, Figure 11c illustrates that the improvement in the water-balance simulation performance of Eco-XAJ-UH, as compared to XAJ-UH, is relative to the NDVI, with more noticeable improvement when the NDVI exceeds 0.68. In Figure 11d, the Eco-XAJ-LR model shows an improvement in water balance simulation as compared to the XAJ-LR model, with only two events having negative values of  $\Delta pBIAS$  near 0. Moreover, similar to the Eco-XAJ-UH model, when the NDVI exceeds 0.68, the Eco-XAJ-LR model demonstrates a noticeable enhancement in water balance simulation as compared to the XAJ-LR model.

In Figure 11, it is evident that the performance improvement from the XAJ model to the Eco-XAJ model is related to the NDVI. When the NDVI is below 0.68, the XAJ-UH model underestimates the discharge, which implies that the XAJ-UH model overestimates evapotranspiration. Correspondingly, the XAJ-UH model underestimates evapotranspiration when the NDVI is above 0.68. Meanwhile, the XAJ-LR model generally overestimates discharge and underestimates evapotranspiration. The deviation becomes more pronounced when the NDVI is above the threshold of 0.68. For the two Eco-XAJ models, the pronounced

performance improvement, as compared to the XAJ models, occurs when the NDVI exceeds 0.68. This threshold is consistent with the inflection point observed in Figure 4a,c. This indicates that the Eco-XAJ models, by dynamically adjusting parameter K, simulate more reasonable evapotranspiration, leading to more accurate simulated discharge.



**Figure 11.** (a,c) Comparison the  $pBIAS$  of the Eco-XAJ models and the XAJ models during low-flow periods. (b,d)  $\Delta pBIAS$  of the Eco-XAJ models and the XAJ models during low-flow periods, where  $\Delta pBIAS = |pBIAS_{XAJ}| - |pBIAS_{Eco-XAJ}|$ .

## 5. Conclusions

This study developed the eco-hydrological model Eco-XAJ to account for the vegetation changes in the Ou River basin. In the Eco-XAJ model, a regression relationship between the parameter K in the XAJ model and the NDVI was established. This method dynamically adjusts the model parameters to account for vegetation changes. The main conclusion can be drawn as follows:

(1) The simulation accuracy of the Eco-XAJ model is generally better than that of the original model. The differences between the two models are mainly observed in low-discharge simulations, with relatively minor differences in high-discharge simulations. The Eco-XAJ model improves the accuracy in the simulation of discharge below  $1000 \text{ m}^3/\text{s}$ .

(2) In the dry season, the advantage of the Eco-XAJ model lies in its ability to overcome the peak overestimation and erroneous peak simulations present in the XAJ model. The advantage in overcoming peak overestimation is most evident in the simulation of unimodal peaks, while the advantage in correcting erroneous peak simulations is reflected in the recession phase after flood events. When the XAJ model produces unreasonable simulations throughout the dry season, the improvements brought by the Eco-XAJ model are limited and not significant. In contrast, when the results of the XAJ model are relatively reasonable during the dry season, the overall performance of the Eco-XAJ model shows slight improvement.

(3) During drought events, the *pBIAS* of the Eco-XAJ model is typically lower than that of the original model. This advantage is more pronounced in the Eco-XAJ-LR model. Considering vegetation changes, the model's performance has improved from the perspective of water balance, especially for discharge simulation of drought events with a high NDVI.

It is worth noting that in regions affected by seasonal fires or intensive agriculture, vegetation may undergo rapid changes in both spatial extent and composition. The monthly NDVI may not respond quickly enough to these kinds of land cover changes. As a result, this model may not be able to capture this change. In further studies, to settle the problem, daily vegetation data such as Enhanced Vegetation Index (EVI) or LAI can be introduced into the model to capture more detailed vegetation changes. To incorporate the frequency and intensity of agricultural activities or fires into the eco-hydrological model can also help get rid of this limitation.

**Author Contributions:** Conceptualization, Z.B.; Methodology, J.S.; Software, Y.K., Q.W. and W.Y.; Formal analysis, H.G.; Investigation, H.G.; Data curation, Y.K. and Q.W.; Writing—original draft, Y.K., Z.B. and D.M.; Writing—review & editing, H.G. and D.M.; Supervision, H.G., Z.B. and D.M.; Project administration, H.G.; Funding acquisition, Z.B. All authors have read and agreed to the published version of the manuscript.

**Funding:** This study is financially supported by National Nature Science Foundation of China (52209036), Natural Science Foundation of Zhejiang Province (LZJWY22D010001), Natural Science Foundation of Ningbo Municipality (2022J160), and Wenzhou Annual Project of Philosophy and Social Science Planning (24WSK166YBM).

**Data Availability Statement:** The data supporting this study's findings are available on request from the corresponding author.

**Conflicts of Interest:** The authors declare no conflicts of interest.

## Appendix A

**Table A1.** Parameters to be calibrated and sensitive parameters (marked with bold) of the XAJ model.

Module	Parameter	Physical Meaning	Range
Evapotranspiration	<b>K</b>	Ratio of potential evapotranspiration to pan evaporation	0.7–1.1
	C	Evapotranspiration coefficient of the deeper soil layer	0.01–0.05
Runoff generation	WUM	Soil water tension capacity of the upper layer	0–100
	WLM	Soil water tension capacity of the lower layer	0–100
	WDM	Soil water tension capacity of the deep layer	0–50
	B	Exponential of the distribution to water tension capacity	0.1–0.8
	IMP	Percentage of impervious and saturated areas in the catchment	0–0.05
Runoff separation	<b>SM</b>	Free water capacity of the surface soil layer	0–100
	EX	Exponent of the free water capacity curve influencing the development of the saturated area	0–2.5
Routing	<b>KI</b>	Outflow coefficients of soil's free water storage to interflow	0–0.7
	<b>KG</b>	Outflow coefficients of soil's free water storage to groundwater	0–0.7
	<b>CI</b>	Recession constants of the interflow	0–1
	CG	Recession constants of the groundwater storage	0–1
Routing (UH)	<b>UH</b>	Unit hydrograph	0–50
	L	Lag time	Defined
Routing (LR)	<b>CS</b>	Recession constants of the surface flow	0–1



**Table A2.** Evaluations of the simulation with the parameter sets calibrated in the XAJ model.

Period	Metric	Model	
		XAJ-UH	XAJ-LR
Calibration	NSE	0.643	0.569
	$r$	0.809	0.767
	$pBIAS$ %	−2.2	11.6
Validation	NSE	0.623	0.616
	$r$	0.815	0.798
	$pBIAS$ %	−21.6	−8.9

## References

- Zhang, G.; He, Y.; Huang, J.; Fu, L.; Han, D.; Guan, X.; Zhang, B. Divergent Sensitivity of Vegetation to Aridity between Drylands and Humid Regions. *Sci. Total Environ.* **2023**, *884*, 163910. [[CrossRef](#)] [[PubMed](#)]
- Yang, Y.; Roderick, M.L.; Guo, H.; Miralles, D.G.; Zhang, L.; Fatichi, S.; Luo, X.; Zhang, Y.; McVicar, T.R.; Tu, Z.; et al. Evapotranspiration on a Greening Earth. *Nat. Rev. Earth Environ.* **2023**, *4*, 626–641. [[CrossRef](#)]
- Momiyama, H.; Kumagai, T.; Fujime, N.; Egusa, T.; Shimizu, T. Forest Canopy Interception Can Reduce Flood Discharge: Inferences from Model Assumption Analysis. *J. Hydrol.* **2023**, *623*, 129843. [[CrossRef](#)]
- Lan, T.; Lin, K.; Xu, C.-Y.; Liu, Z.; Cai, H. A Framework for Seasonal Variations of Hydrological Model Parameters: Impact on Model Results and Response to Dynamic Catchment Characteristics. *Hydrol. Earth Syst. Sci.* **2020**, *24*, 5859–5874. [[CrossRef](#)]
- Ma, D.; Xu, Y.-P.; Xuan, W.; Gu, H.; Sun, Z.; Bai, Z. Do Model Parameters Change under Changing Climate and Land Use in the Upstream of the Lancang River Basin, China? *Hydrol. Sci. J.* **2020**, *65*, 1894–1908. [[CrossRef](#)]
- Mendoza, P.A.; Clark, M.P.; Barlage, M.; Rajagopalan, B.; Samaniego, L.; Abramowitz, G.; Gupta, H. Are We Unnecessarily Constraining the Agility of Complex Process-Based Models? *Water Resour. Res.* **2015**, *51*, 716–728. [[CrossRef](#)]
- Espinoza, E.A.; Loritz, R.; Chaves, M.Á.; Bäuerle, N.; Ehret, U. To Bucket or Not to Bucket? Analyzing the Performance and Interpretability of Hybrid Hydrological Models with Dynamic Parameterization. *Hydrol. Earth Syst. Sci.* **2024**, *28*, 2705–2719. [[CrossRef](#)]
- Feng, D.; Liu, J.; Lawson, K.; Shen, C. Differentiable, Learnable, Regionalized Process-Based Models With Multiphysical Outputs Can Approach State-Of-The-Art Hydrologic Prediction Accuracy. *Water Resour. Res.* **2022**, *58*, e2022WR032404. [[CrossRef](#)]
- Höge, M.; Scheidegger, A.; Baity-Jesi, M.; Albert, C.; Fenicia, F. Improving Hydrologic Models for Predictions and Process Understanding Using Neural ODEs. *Hydrol. Earth Syst. Sci.* **2022**, *26*, 5085–5102. [[CrossRef](#)]
- Kraft, B.; Jung, M.; Körner, M.; Koirala, S.; Reichstein, M. Towards Hybrid Modeling of the Global Hydrological Cycle. *Hydrol. Earth Syst. Sci.* **2022**, *26*, 1579–1614. [[CrossRef](#)]
- Wang, C.; Jiang, S.; Zheng, Y.; Han, F.; Kumar, R.; Rakovec, O.; Li, S. Distributed Hydrological Modeling with Physics-Encoded Deep Learning: A General Framework and Its Application in the Amazon. *Water Resour. Res.* **2024**, *60*, e2023WR036170. [[CrossRef](#)]
- Wang, L.; Xu, Y.-P.; Xu, J.; Gu, H.; Bai, Z.; Zhou, P.; Yu, H.; Guo, Y. Increasing Parameter Identifiability through Clustered Time-Varying Sensitivity Analysis. *Environ. Model. Softw.* **2024**, *181*, 106189. [[CrossRef](#)]
- Jin, X.; Jin, Y.; Fu, D.; Mao, X. Modifying the SWAT Model to Simulate Eco-Hydrological Processes in an Arid Grassland Dominated Watershed. *Front. Environ. Sci.* **2022**, *10*, 939321. [[CrossRef](#)]
- McMahon, T.A.; Peel, M.C.; Lowe, L.; Srikanthan, R.; McVicar, T.R. Estimating Actual, Potential, Reference Crop and Pan Evaporation Using Standard Meteorological Data: A Pragmatic Synthesis. *Hydrol. Earth Syst. Sci.* **2013**, *17*, 1331–1363. [[CrossRef](#)]
- Zhang, Y.; Peña-Arancibia, J.L.; McVicar, T.R.; Chiew, F.H.S.; Vaze, J.; Liu, C.; Lu, X.; Zheng, H.; Wang, Y.; Liu, Y.Y.; et al. Multi-Decadal Trends in Global Terrestrial Evapotranspiration and Its Components. *Sci. Rep.* **2016**, *6*, 19124. [[CrossRef](#)]
- Penman, H.L. Natural Evaporation from Open Water, Bare Soil and Grass. *Proc. R. Soc. London. Ser. A Math. Phys. Sci.* **1948**, *193*, 120–145. [[CrossRef](#)]
- Monteith, J.L. Evaporation and Environment. *Symp. Soc. Exp. Biol.* **1965**, *19*, 205–234. [[PubMed](#)]
- Leuning, R.; Zhang, Y.Q.; Rajaud, A.; Cleugh, H.; Tu, K. A Simple Surface Conductance Model to Estimate Regional Evaporation Using MODIS Leaf Area Index and the Penman-Monteith Equation. *Water Resour. Res.* **2008**, *44*, 2007WR006562. [[CrossRef](#)]
- Bai, P.; Liu, X.; Zhang, Y.; Liu, C. Incorporating Vegetation Dynamics Noticeably Improved Performance of Hydrological Model under Vegetation Greening. *Sci. Total Environ.* **2018**, *643*, 610–622. [[CrossRef](#)]
- Zore, A.; Bezak, N.; Šraj, M. The Influence of Rainfall Interception on the Erosive Power of Raindrops under the Birch Tree. *J. Hydrol.* **2022**, *613*, 128478. [[CrossRef](#)]
- Wang, Z.; Liu, Y.; Wang, Z.; Zhang, H.; Chen, X.; Wen, Z.; Lin, Z.; Han, P.; Xue, T. Quantifying the Spatiotemporal Changes in Evapotranspiration and Its Components Driven by Vegetation Greening and Climate Change in the Northern Foot of Yinshan Mountain. *Remote Sens.* **2024**, *16*, 357. [[CrossRef](#)]
- Poozan, A.; William Western, A.; James Burns, M.; Arora, M. Modelling the Interaction between Vegetation and Infiltrated Stormwater. *J. Hydrol.* **2022**, *607*, 127527. [[CrossRef](#)]
- Kaluža, T.; Eslamian, S. Impact of the Development of Vegetation on Flow Conditions and Flood Hazards. In *Handbook of Engineering Hydrology*; CRC Press: Boca Raton, FL, USA, 2014; ISBN 978-0-429-09659-4.

24. Huang, S.; Tang, L.; Hupy, J.P.; Wang, Y.; Shao, G. A Commentary Review on the Use of Normalized Difference Vegetation Index (NDVI) in the Era of Popular Remote Sensing. *J. For. Res.* **2021**, *32*, 1–6. [[CrossRef](#)]
25. Xie, J.; Xu, Y.-P.; Wang, Y.; Gu, H.; Wang, F.; Pan, S. Influences of Climatic Variability and Human Activities on Terrestrial Water Storage Variations across the Yellow River Basin in the Recent Decade. *J. Hydrol.* **2019**, *579*, 124218. [[CrossRef](#)]
26. Wang, L.; Xu, Y.-P.; Gu, H.; Liu, L.; Liang, X.; Chen, S. Revealing Joint Evolutions and Causal Interactions in Complex Eco-Hydrological Systems by a Network-Based Framework. *Hydrol. Earth Syst. Sci. Discuss.* **2024**, *2024*, 1–31. [[CrossRef](#)]
27. Pan, S.; Liu, L.; Bai, Z.; Xu, Y.-P. Integration of Remote Sensing Evapotranspiration into Multi-Objective Calibration of Distributed Hydrology–Soil–Vegetation Model (DHSVM) in a Humid Region of China. *Water* **2018**, *10*, 1841. [[CrossRef](#)]
28. Zhang, P.; Cai, Y.; He, Y.; Xie, Y.; Zhang, X.; Li, Z. Changes of Vegetational Cover and the Induced Impacts on Hydrological Processes under Climate Change for a High-Diversity Watershed of South China. *J. Environ. Manag.* **2022**, *322*, 115963. [[CrossRef](#)]
29. Bai, Z.; Xu, Y.-P.; Pan, S.; Liu, L.; Wang, Z. Evaluating the Performance of Hydrological Models with Joint Multifractal Spectra. *Hydrol. Sci. J.* **2022**, *67*, 1771–1789. [[CrossRef](#)]
30. Hansen, M.C.; Defries, R.S.; Townshend, J.R.G.; Sohlberg, R. Global Land Cover Classification at 1 Km Spatial Resolution Using a Classification Tree Approach. *Int. J. Remote Sens.* **2000**, *21*, 1331–1364. [[CrossRef](#)]
31. Pinzon, J.E.; Pak, E.W.; Tucker, C.J.; Bhatt, U.S.; Frost, G.V.; Macander, M.J. *Global Vegetation Greenness (NDVI) from AVHRR GIMMS-3G+, 1981–2022*; ORNL DAAC: Oak Ridge, TN, USA, 2023. [[CrossRef](#)]
32. Zhao, R.-J. The Xinanjiang Model Applied in China. *J. Hydrol.* **1992**, *135*, 371–381. [[CrossRef](#)]
33. Liu, L.; Gu, H.; Xu, Y.-P.; Zheng, C.; Zhou, P. Real-Time Flood Forecasting via Parameter Regionalization and Blending Nowcasts with NWP Forecasts over the Jiao River, China. *J. Hydrometeorol.* **2023**, *24*, 561–582. [[CrossRef](#)]
34. Chen, H.; Huang, S.; Xu, Y.-P.; Teegavarapu, R.S.V.; Guo, Y.; Nie, H.; Xie, H.; Zhang, L. River Ecological Flow Early Warning Forecasting Using Baseflow Separation and Machine Learning in the Jiaojiang River Basin, Southeast China. *Sci. Total Environ.* **2023**, *882*, 163571. [[CrossRef](#)] [[PubMed](#)]
35. Wigmosta, M.S.; Vail, L.W.; Lettenmaier, D.P. A Distributed Hydrology-Vegetation Model for Complex Terrain. *Water Resour. Res.* **1994**, *30*, 1665–1679. [[CrossRef](#)]
36. Kollat, J.B.; Reed, P.M. Comparing State-of-the-Art Evolutionary Multi-Objective Algorithms for Long-Term Groundwater Monitoring Design. *Adv. Water Resour.* **2006**, *29*, 792–807. [[CrossRef](#)]
37. Kollat, J.B.; Reed, P.M.; Wagener, T. When Are Multiobjective Calibration Trade-Offs in Hydrologic Models Meaningful? *Water Resour. Res.* **2012**, *48*, W03520. [[CrossRef](#)]
38. Bai, P.; Liu, X.; Zhang, Y.; Liu, C. Assessing the Impacts of Vegetation Greenness Change on Evapotranspiration and Water Yield in China. *Water Resour. Res.* **2020**, *56*, e2019WR027019. [[CrossRef](#)]

**Disclaimer/Publisher’s Note:** The statements, opinions and data contained in all publications are solely those of the individual author(s) and contributor(s) and not of MDPI and/or the editor(s). MDPI and/or the editor(s) disclaim responsibility for any injury to people or property resulting from any ideas, methods, instructions or products referred to in the content.